

High-power single-stage thulium-doped superfluorescent fiber source

Z. Y. Hu · P. Yan · Q. Liu · E. C. Ji · Q. R. Xiao ·
M. L. Gong

Received: 6 September 2014 / Accepted: 30 October 2014 / Published online: 7 November 2014
© The Author(s) 2014. This article is published with open access at Springerlink.com

Abstract In this paper, we report a high-power thulium (Tm)-doped superfluorescent fiber source (SFS) in the 2- μm spectral region. The SFS is based on double angle-cleaved facet operation and uses a simple single-stage geometry. The copropagating amplified spontaneous emission (ASE) yields a maximum output of 20.7 W at a center wavelength of 1,960.7 nm, with a full width at half maximum (FWHM) of ~ 45 nm. The counterpropagating ASE yields a maximum output of 25.2 W at a center wavelength of 1,948.2 nm, with a FWHM of ~ 50 nm. The maximum combined output of the SFS is as much as 45.9 W, which corresponds to a slope efficiency of 38.9 %. In addition, a model of the ~ 2 μm SFS in Tm-doped silica fibers pumped at ~ 790 nm is developed, and the influence of fiber length and end-facet reflectivity on the ASE output performance and the parasitic lasing threshold are studied numerically.

1 Introduction

Superfluorescent fiber sources (SFSs) have the advantages of broad emission spectra, high output powers, high overall conversion efficiencies, and excellent spatial coherence [1, 2]. The combination of these characteristics makes SFSs suitable for applications in rotation sensing, pumping of Raman lasers, medical imaging, and optical coherence domain reflectometry [3, 4]. Therefore, SFSs have become the focus of major research worldwide.

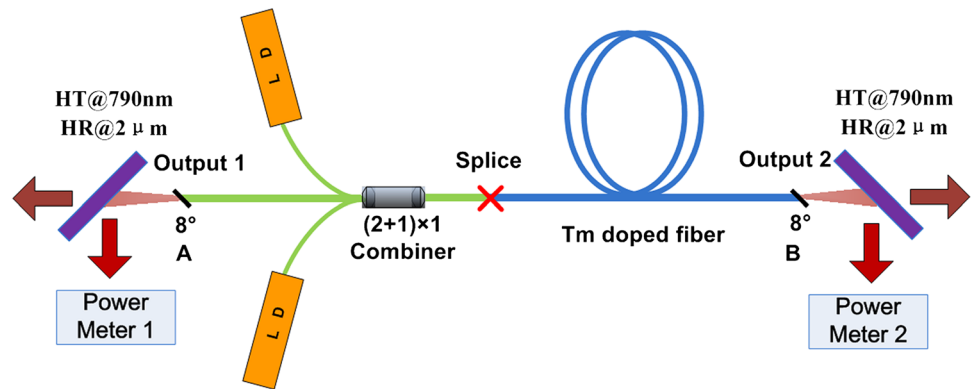
In the past few years, rapid progress has been made in scaling of the amplified spontaneous emission (ASE) output. For a high-power SFS in the 1- μm spectral region [5–9], Schmidt et al. [9] reported a narrow-band SFS with maximum output power of 697 W at a center wavelength of 1,030 nm using a two-stage master oscillator power amplifier (MOPA) configuration. In comparison with SFSs in the 1- μm spectral region, few studies have been reported to date on high-power broadband thulium (Tm)-doped SFSs in the 2- μm spectral region [10–12]. In 2008, Shen et al. [13] demonstrated a broadband Tm-doped fiber SFS with a single-ended output power of 11 W using a free-space pump configuration. The slope efficiency was 38 %, and the full width at half maximum (FWHM) bandwidth was 36 nm. Recently, Liu et al. [14] reported a 122-W broadband superfluorescence output using a MOPA configuration, with a wavelength range that spanned from 1,935 to 2,075 nm and a FWHM bandwidth of 25 nm. Obviously, a MOPA scheme can produce a higher ASE output than a single-stage SFS generation scheme. However, the main drawback of the MOPA scheme is that it is rather complex. It requires two kinds of fibers (and their associated pump sources) and one or more Faraday isolators to provide the required degree of attenuation of feedback to both the seed and the amplifier. In contrast, a single-stage SFS generation scheme needs fewer elements and requires less space, so it is both simpler and more compact. In addition, it is not easy to realize an all-fiber SFS for a MOPA scheme because of the destructive effect of the strong backward ASE on the pump source and the other optical components.

In this paper, we report a simple approach for scaling of the output power from a Tm-doped SFS using a single-stage configuration in combination with a double angle-cleaved facet geometry to reduce the feedback from the fiber-end facets and provide effective suppression of the

Z. Y. Hu · P. Yan · Q. Liu · E. C. Ji · Q. R. Xiao · M. L. Gong (✉)
Center for Photonics and Electronics, Department of Precision
Instrument, Tsinghua University, Beijing 100084, China
e-mail: gongml@mail.tsinghua.edu.cn

Z. Y. Hu
e-mail: huzhenyue@gmail.com

Fig. 1 Schematic of the Tm-doped SFS setup



parasitic lasing. With high surface and splicing point quality, the SFS generates maximum output powers of 20.7 and 25.2 W from the double ends. The maximum combined output of the SFS is as much as 45.9 W, which corresponds to a slope efficiency of 38.9 %. To the best of our knowledge, this is by far the highest power produced by a single-stage Tm-doped SFS. Also, a model of the $\sim 2\text{-}\mu\text{m}$ SFS using Tm-doped silica fibers pumped at $\sim 790\text{ nm}$ is developed, and it is interesting to find that both the optical feedback and the active fiber length are of great importance to the power scalability of the SFS. It is shown that multi-hundred-watt ASEs can be achieved using this scheme.

2 Experimental setup and results

The experimental arrangement used for the high-power Tm-doped SFS is shown schematically in Fig. 1. The active fiber of the SFS is a 3-m-long Tm-doped double-clad silica fiber with absorption of 4 dB m^{-1} at 790 nm. The active fiber core has a diameter of $25\text{ }\mu\text{m}$ and a numerical aperture (NA) of 0.09, and the inner cladding has a diameter of $400\text{ }\mu\text{m}$ and a NA of 0.46. Two fiber-pigtailed multimode diodes (LDs) emitting at 790 nm are used as the pump source with a fiber core diameter of $200\text{ }\mu\text{m}$, NA of 0.22, and total output power of 144 W. In the $(2 + 1) \times 1$ combiner, which was made in our laboratory, the two input fibers have core and cladding diameters of 200 and $220\text{ }\mu\text{m}$, respectively, with an NA of 0.22. Additionally, the signal fiber has core and cladding diameters of 25 and $400\text{ }\mu\text{m}$, respectively. The average coupling efficiency of the two ports is 97.1 %. The active fiber and the combiner are cooled to $\sim 10\text{ }^\circ\text{C}$ in a water-cooled heat sink to promote efficient “two-for-one” cross-relaxation.

To obtain the high-power ASE output, the feedback from the fiber-end facets must be reduced. Fresnel reflection is the main physical origin of the optical feedback from the fiber-end facets, and the most common method used to reduce this feedback is the angle-cleaved facet, which

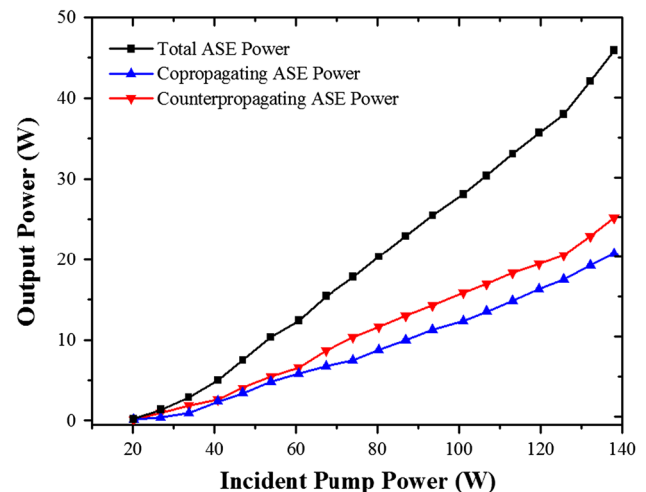
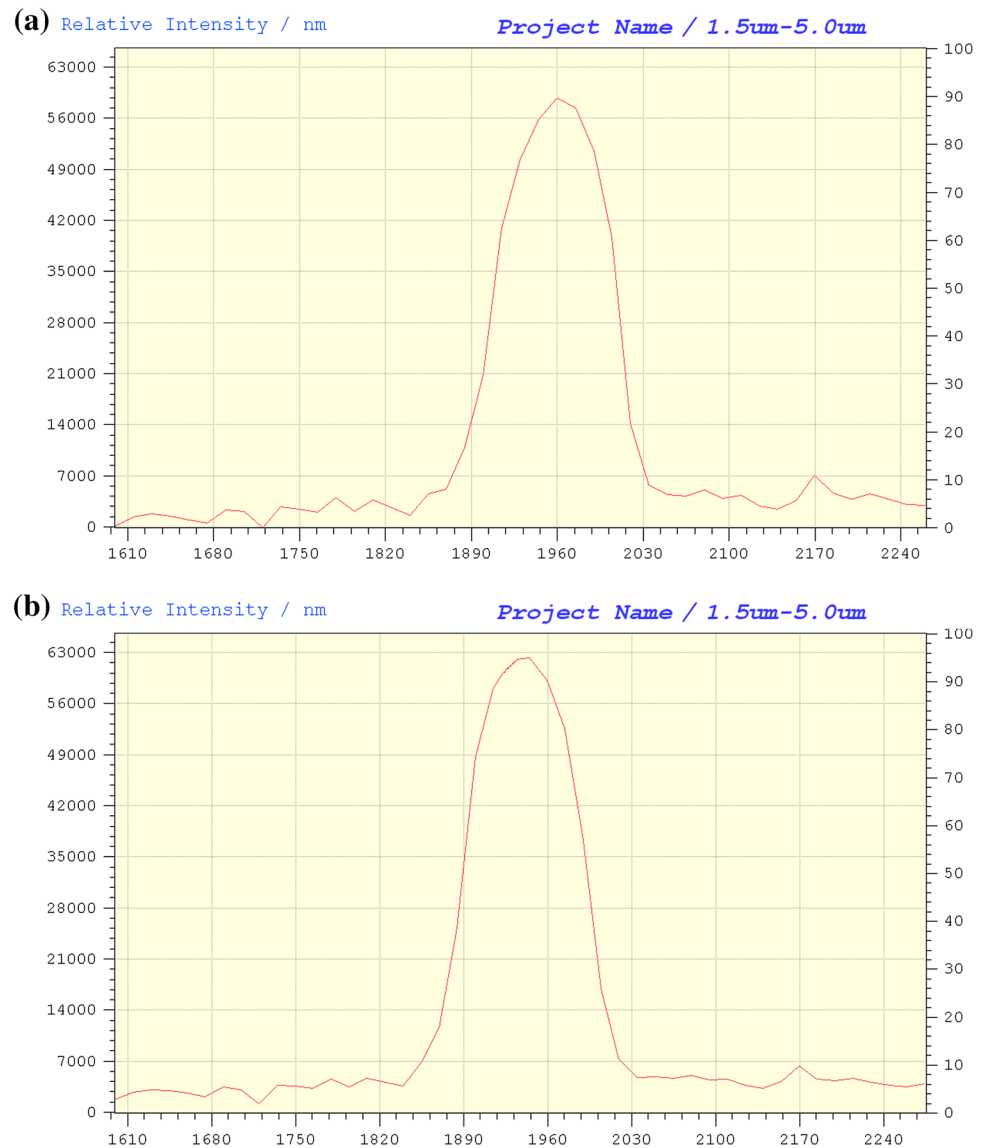


Fig. 2 Experimental ASE output power versus incident pump power for the $\sim 8^\circ$ angle-cleaved two-ended configuration

can reduce the end-faced reflectivity to 50–60 dB. In our experiments, the two output ends of the SFS are angle-cleaved at $\sim 8^\circ$ to produce very low feedback. The fiber end face reflectivity in the absence of defects is approximately 55 dB (3.16×10^{-6}) [8]. Scratches and indentations on the core at the fiber-end facets may cause optical performance degradation [15, 16]. A microscope is therefore used to examine the features of the fiber facet after the angle-cleaving process. A fused splice point exists between the combiner and the active fiber, and this splice point would generate serious optical feedback if it was not fused well. In addition, the fiber length is of great importance for the SFS power scalability, and we need to consider both the output power and the efficiency to choose a suitable fiber length; this process is described in the discussion section.

Two dichroic mirrors are used to separate the pump light from the ASE, and the ASE output power is measured using two power meters (Ophir Nova II: FL250A-LP1-SH-V1 and Coherent: Model PM30V1) at each end simultaneously. The ASE output power versus

Fig. 3 Emission spectra for the Tm-doped SFS: **a** copropagating ASE, and **b** counterpropagating ASE



incident pump power characteristics are plotted in Fig. 2. When the pump power is more than 18 W, the SFS begins to generate an ASE output. The maximum ASE output powers for the copropagating (in the same direction as the direction of pump light propagation) and counterpropagating (in the opposite direction to the direction of pump light propagation) beams are 20.7 and 25.2 W, respectively. The total ASE output power is 45.9 W with an incident pump power of 138 W. The slope efficiencies for the copropagating and counterpropagating beams are 17.5 and 21.4 %, respectively. The slope efficiency of the total ASE output power is 38.9 %, and the optical–optical efficiency is 33.3 % with an incident pump power of 138 W. In comparison to the copropagating ASE, the counterpropagating ASE has greater slope efficiency. This is because the copropagating ASE is reabsorbed in the low pump-power

region, and part of that power is then transformed into the counterpropagating ASE.

The ASE spectra are measured using a spectral analyzer (Spectral Products SM301-EX: CROP35010EV). Note that increasing the pump power will result in the onset of lasing, as confirmed by the sharp peaks in the ASE spectrum. Figure 3a shows the emission spectrum for the copropagating ASE with an output power of 20.7 W, and Fig. 3b shows the emission spectrum for the counterpropagating ASE with an output power of 25.2 W. The counterpropagating ASE is shown to be blueshifted in comparison to the copropagating ASE. The central wavelength of the copropagating ASE is 1,960.7 nm, spanning from 1,890 to 2,030 nm with a FWHM of ~45 nm, whereas the central wavelength of the counterpropagating ASE is 1,948.2 nm, spanning from 1,860 to 2,030 nm with a FWHM of ~50 nm.

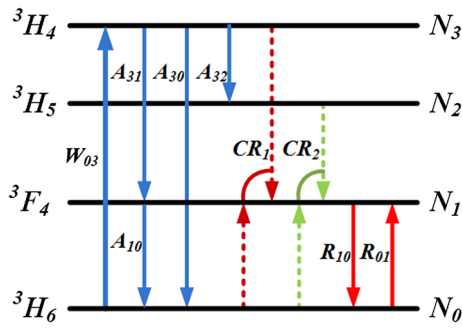


Fig. 4 Schematic view of the four lowest energy levels in the Tm^{3+} ions

3 Discussion

In our experiments, it is shown that a high-power SFS can be realized. Theoretical modeling and simulations are important in investigation of the characteristics of SFSs and subsequent optimization of the SFS parameters for practical systems. A few theoretical models have been reported for the Tm-doped SFS [17–19] without consideration of cross-relaxation (CR). It has been determined that high efficiency can be attained by diode pumping of the ${}^3H_6 \rightarrow {}^3H_4$ transition in combination with high Tm-doping concentrations that enable beneficial interionic CR.

In the model, the ${}^3H_6 \rightarrow {}^3H_4$ transition is chosen for the pumping scheme, and the energy level diagram of Tm^{3+} is shown in Fig. 4. Because the lifetime of the 3H_5 energy level is quite short when compared with the other three energy levels, N_2 and CR_2 both become zero. It is assumed that the pump power is below the laser threshold power, so no laser beams are propagating in the fiber. Based on Jackson’s method [20], the rate equations in Tm-doped SFSs can be expressed using the following equations:

$$\begin{cases} N \approx N_0 + N_1 + N_3 \\ \frac{dN_3}{dt} = W_{03}N_0 - CR_1 - (A_{32} + A_{31} + A_{30})N_3 \\ \frac{dN_1}{dt} = A_{31}N_3 - (R_{10} + A_{10})N_1 + R_{01}N_0 + 2CR_1 \\ \frac{dN_0}{dt} = (R_{10} + A_{10})N_1 - CR_1 - (R_{01} + W_{03})N_0 + A_{30}N_3 \\ CR_1 = k_{3101}N_3N_0 - k_{1013}N_1^2 \end{cases}, \quad (1)$$

where N_0 , N_1 , and N_3 are the population densities of the 3H_6 , 3F_4 , and 3H_4 energy levels, respectively (N is the doping concentration distribution and is assumed to be a

constant); W_{03} represents the pumping rate from 3H_6 to the 3H_4 energy level; A_{ij} represents the spontaneous transition rate from energy level i to level j ; R_{ij} represents the amplified stimulated transition rate from energy level i to level j ; and k_{3101} and k_{1013} represent the CR coefficients.

The ASE spectrum is divided into K channels with a central wavelength of λ_{ai} ($i = 1, 2, \dots, K$), and even spacing of $\Delta\lambda$. Therefore, W_{03} and R_{ij} can be defined by:

$$\begin{cases} W_{03} = \frac{n\lambda_p\sigma_a(\lambda_p)}{hcA_{core}}\Gamma_p(P_p^+(z) + P_p^-(z)) \\ R_{10} = \sum_{i=1}^K \frac{n\lambda_{ai}\sigma_e(\lambda_{ai})}{hcA_{core}}\Gamma_{ai}(P_{ai}^+(z) + P_{ai}^-(z)), \\ R_{01} = \sum_{i=1}^K \frac{n\lambda_{ai}\sigma_a(\lambda_{ai})}{hcA_{core}}\Gamma_{ai}(P_{ai}^+(z) + P_{ai}^-(z)) \end{cases}, \quad (2)$$

where A_{core} is the cross-sectional area of the core; n is core refractive index; c is the speed of light in a vacuum; h is the Planck constant; $\sigma_{e,a}(\lambda_p)$ are the emission and absorption cross sections of the pump light, respectively; $\sigma_{e,a}(\lambda_{ai})$ are the emission and absorption cross sections of the i th ASE light beam, respectively; $\Gamma_{p,ai}$ are the pump and ASE light power filling distributions, respectively; $P_p^\pm(z)$ are the pump powers in the forward ($z = 0$ to $z = L$) and backward ($z = L$ to $z = 0$) directions, respectively; L is the fiber length; and $P_{ai}^\pm(z)$ are the i th ASE light powers in the forward and backward directions, respectively, and can be described as follows:

$$\begin{cases} \pm \frac{dP_p^\pm(z)}{dz} = [N_1\sigma_e(\lambda_p) - N_0\sigma_a(\lambda_p)]\Gamma_p P_p^\pm(z) - \alpha_p P_p^\pm(z) \\ \pm \frac{dP_{ai}^\pm(z)}{dz} = [N_1\sigma_e(\lambda_{ai}) - N_0\sigma_a(\lambda_{ai})]\Gamma_{ai} P_{ai}^\pm(z) - \alpha_{ai} P_{ai}^\pm(z) + 2\sigma_e(\lambda_{ai})N_1 \frac{hc^2}{\lambda_{ai}^3} \Delta\lambda \end{cases}, \quad (3)$$

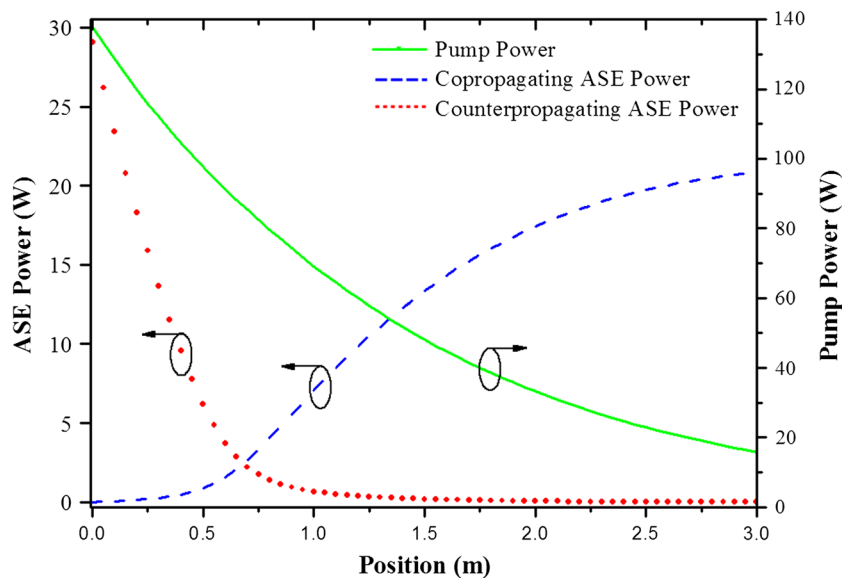
where $\alpha_{p,ai}$ are the pump and the signal of the i th ASE light loss factors, respectively.

By assuming that the pump light reflectivity at each end of the fiber is zero and that the reflectivity is the same for the whole ASE spectrum, the boundary conditions can be expressed as:

$$\begin{cases} P_p^+(0) = P_{in}^+ \\ P_p^-(L) = P_{in}^- \\ P_{ai}^+(0) = R_1 P_{ai}^-(0) \\ P_{ai}^-(L) = R_2 P_{ai}^+(L) \end{cases}, \quad (4)$$

in which P_{in}^\pm are the incident pump powers in the forward and backward directions, respectively, and R_1 and R_2

Fig. 5 Power distributions along the fiber length for the pump, the copropagating ASE, and the counterpropagating ASE for $P_{\text{in}}^+ = 138$ W, $R_1 = R_2 = 55$ dB, and $L = 3$ m



are the reflectivities of the ASE light at $z = 0$ and $z = L$, respectively.

For a continuous-wave ASE system, the population densities of each energy level remain steady, and thus, $\frac{dN_3}{dr} = \frac{dN_1}{dr} = \frac{dN_0}{dr} = 0$ in (1). Based on the theoretical ASE model composed of (1)–(3), and boundary conditions of (4), we can obtain individual power and population density distributions along the axial direction by discretization into frequency and spatial intervals and performing subsequent iterations until satisfactory convergence of the output parameter occurs by using the fourth-order Runge–Kutta method. The frequency interval is chosen such that it spans the whole measured cross section of data between the corresponding wavelengths of 1,600 and 2,300 nm [21], which means that the spectral resolution of the calculation is approximately 1 nm. In this paper, we assume that both ends of the fiber are processed by the same method, that the reflectivities of the two ends are equal, and that the pump light only propagates in the forward direction. Results for backward pumping and bidirectional pumping regimes and for different reflectivities at the fiber ends can be obtained in a similar manner. The parameters used in the simulation are listed as follows: $\lambda_p = 790$ nm, $c = 3 \times 10^8$ m s $^{-1}$, $n = 1.458$, $h = 6.626 \times 10^{-34}$ J s, $A_{\text{core}} = 491$ μm^2 , $\Gamma_{\text{ai}} = 0.8$, $\Gamma_p = 3.9 \times 10^{-3}$, $P_{\text{in}}^- = 0$, $\alpha_p = 1.2 \times 10^{-2}$ m $^{-1}$, $\alpha_{\text{ai}} = 2.3 \times 10^{-2}$ m $^{-1}$, $k_{3101} = 3 \times 10^{-23}$, $k_{1013} = 0.084k_{3101}$, $N = 3.54$ wt%, $A_{32} = 9.86$ ms $^{-1}$, $A_{31} = 50.7$ ms $^{-1}$, $A_{30} = 9.86$ ms $^{-1}$, and $A_{10} = 2.99$ ms $^{-1}$. Use of 100 samples along the length of the fiber and <1,000 iteration steps can produce accurate results, and the execution only takes a few minutes on a personal computer.

When the incident pump power is 138 W, the reflectivity at each end is 55 dB, and the fiber length is 3 m, the

resulting pump and ASE power distributions along the length of the fiber are as shown in Fig. 5. For the counterpropagating case, the power shows a nearly exponential increase, with a maximum power of 29 W at the output facet ($z = 0$). In the copropagating case, the power emerges with an exponential-like rise at $z < 1$ m and then increases slowly to its maximum output of 20 W at $z = 3$ m. The reason for this behavior is that the pump power is not large enough in the appropriate region along the fiber, so both the inverted population and the gain decrease, and as a result, the ASE power increases slowly. The total ASE output is 49 W, which is roughly commensurate with our experimental result of 45.9 W.

As mentioned above, the lasing threshold level determines the maximum available output from an ASE source. To obtain a high-power ASE output, it is therefore necessary to predict the lasing threshold. Based on our SFS model, the frequency-dependent gain can be calculated, and then, the maximum of the frequency-dependent gain is compared with the cavity loss. If these values are equal, this means that the SFS is above the lasing threshold [1, 8]. For the given Tm-doped fiber, the lasing threshold is mainly determined by the reflection at the fiber ends and the fiber length.

First, we assume that the fiber length is finite and that the reflectivity is the same at both ends. To obtain the maximum ASE output with different reflectivities at the fiber ends, we calculate the maximum pump power when lasing is generated. Figure 6 shows the maximum pump power at $L = 3$ m with different reflectivities at the fiber ends. Obviously, the maximum pump power increases with decreasing reflectivity. Within the limit, parasitic lasing would not be generated under any circumstances. When the reflectivity is

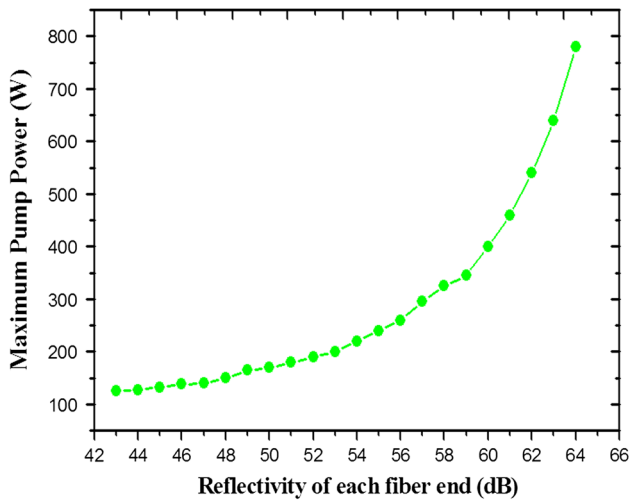
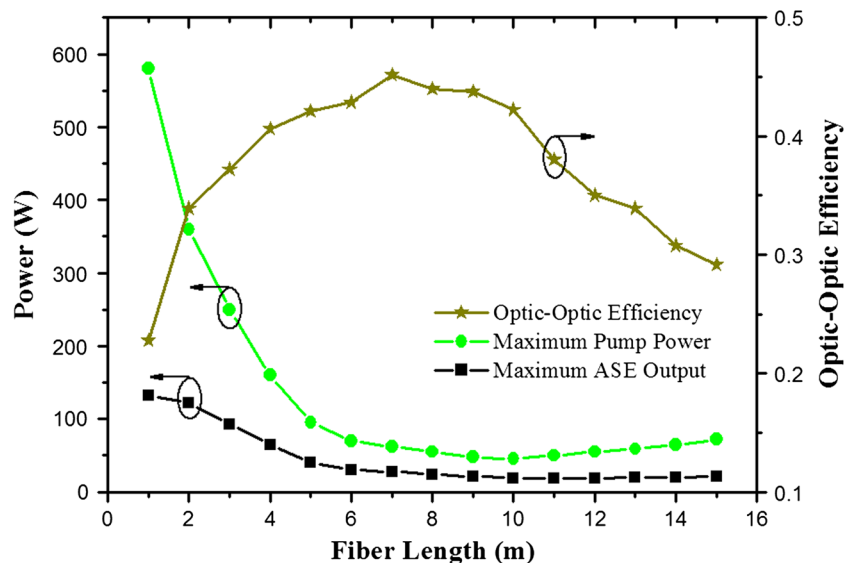


Fig. 6 Maximum pump power versus reflectivity of each fiber end for $L = 3$ m

55 dB, the maximum pump power is approximately 235 W, and this power is considerably larger than our experimental maximum pump power of 138 W.

Second, because of the absorption and loss of the signal and pump powers in the fiber, the maximum pump power and the ASE output will change when the fiber length changes. The effect of the fiber length on the ASE source is shown in Fig. 7, assuming that the reflectivity at each fiber end is 55 dB. In general, the maximum pump power decreases when the fiber length increases. However, the maximum pump power increases slowly when the fiber length is longer than 11 m. Because the pump power is not high enough at the far pump end, the ASE self-absorption

Fig. 7 Maximum pump power, maximum ASE output, and optical–optical efficiency versus fiber length for $R_1 = R_2 = 55$ dB



becomes serious. Also, the ASE output power and the relevant optical–optical efficiency at the maximum pump power are plotted for different fiber lengths. The maximum ASE output could be as high as 142 W when the fiber length is 1 m, but the optical–optical efficiency is just 23.2 %. When the fiber length increases from 5 to 9 m, the efficiency is relatively high and changes slowly at about 42–45 %, but the maximum ASE output is just 42 W. The fiber length is therefore chosen to be 3 m by considering the ASE output and the efficiency in the presented experiment.

4 Conclusion

In this paper, we have demonstrated broadband ASE in the 2- μm spectral region based on a Tm-doped double-clad silica fiber, with a single-stage double angle-cleaved facet configuration. The maximum powers for the counter-propagating and copropagating beams are 25.2 and 20.7 W, respectively, with an incident pump power of 138 W. The total ASE output power from the fiber is 45.9 W, which corresponds to a total optical–optical efficiency of 33.3 % and a slope efficiency of 38.9 %.

By solving a set of frequency-dependent rate equations, a model of the ASE system is developed, the power distributions along the fiber length for the pump, the copropagating ASE and the counterpropagating ASE are plotted, and the theoretical ASE output is found to be roughly commensurate with our experimental result. For the given fiber, the influences of the fiber facet reflectivity and the fiber length on the laser threshold are discussed, and we can see that these parameters play important roles in the ASE output.

Acknowledgments This research was partially supported by the National Natural Science Foundation of China (Grant No. 61307057), the State Key Laboratory of Tribology, Tsinghua University, China (Grant No. SKLT12B08), and the China Postdoctoral Science Foundation (Grant Nos. 2012M520258 and 2013T60109).

Open Access This article is distributed under the terms of the Creative Commons Attribution License which permits any use, distribution, and reproduction in any medium, provided the original author(s) and the source are credited.

References

1. I.N. Duling III, R. Moeller, W.K. Burns, C.A. Villarruel, L. Goldberg, E. Snitzer, H. Po, *IEEE J. Quantum Electron.* **27**, 995 (1991)
2. P.F. Moulton, G.A. Rines, E.V. Slobodtchikov, K.F. Wall, G. Frith, B. Samson, A.L.G. Carter, *IEEE J. Sel. Top. Quantum Electron.* **15**, 85 (2009)
3. B.E. Bouma, L.E. Nelson, G.J. Tearney, D.J. Jones, M.E. Brezinski, J.G. Fujimoto, *J. Biomed. Opt.* **3**, 76 (1998)
4. K. Oh, T. Morse, A. Kilian, *Meas. Sci. Technol.* **9**, 1409 (1998)
5. P. Wang, J. Sahu, W. Clarkson, *Opt. Lett.* **31**, 3116 (2006)
6. V. Filippov, Y. Chamorovskii, J. Kerttula, K. Golant, M. Pessa, O. Okhotnikov, *Opt. Express* **16**, 1929 (2008)
7. S.C. Tsai, T.C. Tsai, P.C. Law, Y.K. Chen, *IEEE Photonics Technol. Lett.* **15**, 197 (2003)
8. Q.R. Xiao, P. Yan, Y.P. Wang, J.P. Hao, M.L. Gong, *Appl. Opt.* **50**, 1164 (2011)
9. O. Schmidt, M. Rekas, C. Wirth, J. Rothhardt, S. Rhein, A. Kliner, M. Strecker, T. Schreiber, J. Limpert, R. Eberhardt, *Opt. Express* **19**, 4421 (2011)
10. Y.H. Tsang, T.A. King, D.K. Ko, J. Lee, *J. Mod. Opt.* **53**, 991 (2006)
11. A. Halder, M.C. Paul, N. Shahabuddin, S. Harun, N. Saidin, S. Damanhuri, H. Ahmad, S. Das, M. Pal, S.K. Bhadra, *IEEE Photonics J.* **4**, 14 (2012)
12. Z. Li, A. Heidt, N. Simakov, Y. Jung, J. Daniel, S. Alam, D. Richardson, *Opt. Express* **21**, 26450 (2013)
13. D. Shen, L. Pearson, P. Wang, J. Sahu, W. Clarkson, *Opt. Express* **16**, 11021 (2008)
14. J. Liu, K. Liu, F.Z. Tan, P. Wang, *IEEE J. Sel. Top. Quantum Electron.* **20**, 1 (2014)
15. E. Avram, W. Mahmood, M. Ozer, *J. Lightwave Technol.* **20**, 634 (2002)
16. P. Chanclou, M. Thual, J. Iostec, *Appl. Opt.* **40**, 458 (2001)
17. K. Oh, A. Kilian, P. Weber, L. Reinhart, Q. Zhang, T. Morse, *Opt. Lett.* **19**, 1131 (1994)
18. P. Peterka, B. Faure, W. Blanc, M. Karasek, B. Dussardier, *Opt. Quantum Electron.* **36**, 201 (2004)
19. M. Gorjan, T. North, M. Rochette, *J. Opt. Soc. Am. B* **29**, 2886 (2012)
20. S.D. Jackson, T.A. King, *J. Lightwave Technol.* **17**, 948 (1999)
21. S.D. Jackson, *Proc. SPIE* **7686**, 768608 (2010)